applied sciences

MDPI

Article

Research on the Control Problem of Autonomous Underwater Vehicles Based on Strongly Coupled Radial Basis Function Conditions

Qinghe Zhang [1], Longchuan Guo [1,*], Md Abrar Hasan Sohan [2] and Xiaoqing Tian [1,3,*]

[1] School of Mechanical Engineering, Hangzhou Dianzi University, Hangzhou 310018, China; 211010034@hdu.edu.cn
[2] School of International Education, Hangzhou Dianzi University, Hangzhou 310018, China; sohanbracu2200@gmail.com
[3] Ocean College, Zhejiang University, Zhoushan 316021, China
* Correspondence: glc1988@126.com (L.G.); tianxiaoqing@zju.edu.cn (X.T.)

Abstract: This paper addresses tracking control problems for autonomous underwater vehicle (AUV) systems with coupled nonlinear functions. For the first time, the radial basis function (RBF) is applied to the model reference adaptive control system, and the vehicle horizontal plane model is proposed. When the AUV movement is affected by the driving force, ocean resistance, and the force generated by the water current, the expected output of the AUV's system is difficult to meet the expectations, making the AUV trajectory tracking problems challenging. There are two main options for finding suitable controllers for AUVs. The first is making the AUV model achieve better stability using a more complex controller. The second is the simpler controller structure, which can ensure faster system feedback. The RBF and model reference adaptive control (MEAC) system are combined to increase the number of hidden layers, increasing the AUV tracking stability. Because the embedded computing module of an AUV is a bit limited, 31 hidden layers are chosen to simplify the controller structures. A couple of Lyapunov functions are designed for the expected surge and sway velocities, and the vehicle tracking error gradually converges to (0,0). The controller design results are imported into the AUV actuator model by software, and after 0.64 s, the AUV tracking error is less than 1%. At last, the vehicle tracking experiments were carried out, showing that after 0.5 s, the AUV tracking error was less than 1%.

Keywords: tracking system; uncertain nonlinear systems; AUV; RBF; MRAC

check for updates

Citation: Zhang, Q.; Guo, L.; Sohan, M.A.H.; Tian, X. Research on the Control Problem of Autonomous Underwater Vehicles Based on Strongly Coupled Radial Basis Function Conditions. *Appl. Sci.* **2023**, *13*, 7732. https://doi.org/10.3390/app13137732

Academic Editor: Zhaoyu Wei

Received: 29 May 2023
Revised: 19 June 2023
Accepted: 28 June 2023
Published: 29 June 2023

Copyright: © 2023 by the authors. Licensee MDPI, Basel, Switzerland. This article is an open access article distributed under the terms and conditions of the Creative Commons Attribution (CC BY) license (https://creativecommons.org/licenses/by/4.0/).

1. Introduction

With the continuous progress and development of human society, the development and utilization of the ocean are critical. As the most resource-rich place in the world, the sea has always attracted people's exploration. Autonomous underwater vehicles (AUVs) have been the focus of many oceanographic studies in recent decades due to their wide-ranging applications in ocean exploration, ocean mapping, underwater pipeline inspection, and scientific and military missions [1–3]. The development of fluid mechanics also promotes the progress of AUV underwater dynamics analysis [4,5]. Due to the model characteristics of AUV (nonlinearity, coupling, uncertainty), there are many external disturbances underwater in practical applications. Most AUVs are underdriven to reduce weight, which degrades the performance of AUVs [6]. The design of the control system becomes one of the most considerable difficulties in its development. Therefore, it is necessary to study the robust control of underactuated AUVs [7–9].

The autonomous underwater vehicle (AUV) is the latest achievement in the field of marine robot research. Because it does not require human intervention during its work, it dramatically reduces the risk and operating costs of various underwater projects, so it has

received attention from industry and academia. There is increasing attention in [10], which proves that well-designed control systems are necessary. Their limitations are known for existing control techniques such as proportional integral derivative (PID), adaptive control, and model predictive control. In early industrial process control, the system's parameters often changed because it was difficult to establish an accurate mathematical model of the controlled object. PID has many uses due to its simple control technology structure and convenient parameter adjustment, but it is only used in simple control systems [11–13]. The research object of adaptive control is a system whose parameters are not entirely determined, and the environment contains unknown and random factors. However, adaptive control is more complicated and costly than conventional control [14–17]. Model predictive control (MPC) is an optimization-based time domain control method [18]. Compared with most traditional control methods, the distinguishing feature of MPC is its ability to deal systematically with system constraints in controller design [19]. Therefore, it is good at dealing with multi-input and multi-output systems. However, to solve the optimization problem, it needs to iterate at each time step, and the solution to the optimization problem is often time-consuming. The controller's action may have more vital requirements for real-time performance. This will produce a contradiction, a significant shortcoming of the current predictive control model [20–23].

Some researchers did not consider the influence of propeller dynamics when designing AUV control schemes. The operating environment of an AUV is complex, and there are many degrees of freedom to be controlled. Existing control algorithms cannot adapt to environmental changes, weakening control effects. In recent years, the neural network represented by the BP algorithm has gradually become popular with the improvement of computing power. This further drives the control algorithm to become more intelligent. The most attractive property of neural networks is adaptability. Adaptability means the neural network can be appropriately organized and adjusted with the controlled object and environmental conditions through learning. Yuh, J. used an AUV to study the feasibility of the neural network control of underwater vehicles in the presence of unpredictable dynamic changes [24]. Some researchers employ neural networks to approximate the complex AUV hydrodynamics and the difference in required tracking speeds [25]. A three-layer neural network can fit any function, but most neural networks require high computing power and cannot meet the real-time requirements of the controller. Usually, the importance of the AUV model and the low performance of the single-chip microcomputer equipped with ordinary AUVs are ignored. To deal with the complex calculation process of traditional neural networks, the real-time requirements of AUVs for control need to be guaranteed. The RBF neural network is used to compensate for plant nonlinearity adaptively, and it was certified that combining adaptive and robust control allows for acceptable approximation errors due to low-order networks [26].

RBF has a relatively simple recursive process, which can ensure that it can also be deployed on microcontrollers with low computing power. Model-based advanced controller design requires accurate models. However, the actual model may need to be more particular about adapting to different environments. Feedback controllers designed for such situations are not particularly effective, which makes adaptive algorithms more and more popular. The model reference adaptive control (MRAC) framework can artificially construct a reference model to represent the dynamic performance of the desired closed-loop system.

Moreover, it can look for a dynamically adjusted feedback control law so that the closed-loop control performance of the system can be consistent with the performance of the reference model [27,28]. It should be pointed out that this paper uses the RBF neural network as the feedback controller of the MRAC, and the actual error between the output and the reference output serves as the input to the RBF. The backpropagation algorithm is used to continuously adjust the weight coefficients of the hidden layer and the output layer to drive the dynamic trajectory of the AUV to be consistent with the reference trajectory. This design also guarantees the dynamic performance of the proposed controller since the weight coefficients are constantly adjusted.

This paper aims to use a model reference adaptive controller on an AUV system and consider RBF neural networks as the adaptive mechanism. The main contributions of this paper include the following:

- A new adaptive algorithm is proposed to solve the AUV trajectory tracking control problem. Using the proposed RBF adaptive algorithm, the performance and robustness of the tracking control can be significantly improved. Furthermore, its subproblems can be addressed simultaneously in the controller design.
- A horizontal plane model for the AUV is proposed. And, for the underactuated underwater vehicle, which only provides surge force and sway moment, the boundedness of its velocity in the horizontal direction is proved.
- For MRAC tracking control, it is neither feasible nor stable to only consider the control performance due to the influence of the optimal solution quality. Therefore, the proposed MRAC creates a trade-off between computational complexity and control performance, introducing an efficient mechanism for allocating computational resources to AUVs.

This article is organized as follows. The second section introduces the kinematics and dynamics modeling of the robot, the third section tackles the controller design, the fourth section is on the underwater robot model and physical analysis, and the fifth section contains the summary and outlook.

2. Description of Dynamic Modelling of AUV

This section presents a system model of a well-known underactuated underwater robot with six degrees of freedom (6-DOF), as shown in Figure 1.

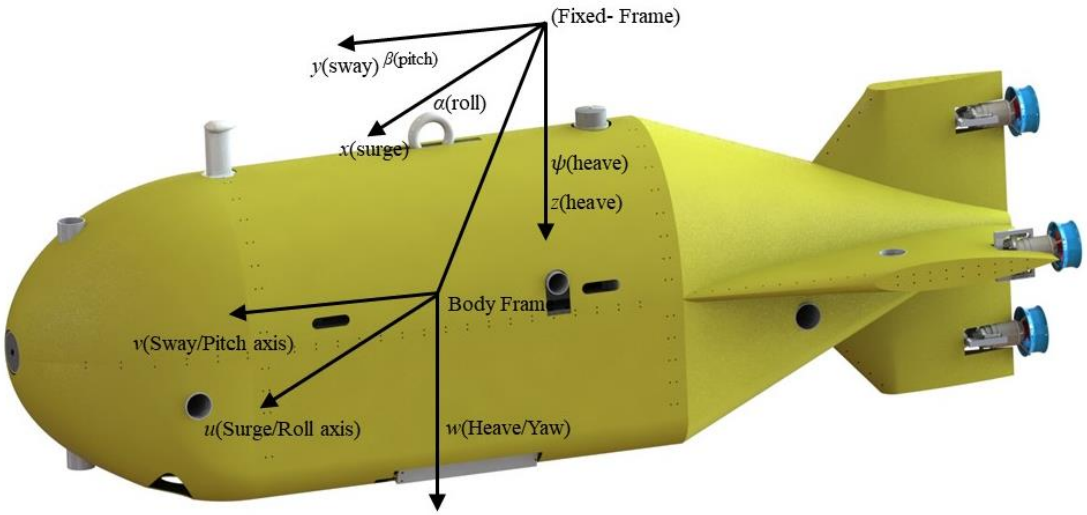


Figure 1. Body-fixed frame and earth-fixed reference frame for an underwater robot.

Underwater vehicles operate in fluids and are subject to a series of forces called hydrodynamics. The ocean currents are more likely to affect underwater vehicles' dynamics and control performance due to their unpredictable speed and direction. For the control problems of underactuated underwater vehicles, it is generally necessary to study their velocity, position, attitude, heading, and degrees of freedom. It is essential to establish a suitable reference frame. A 6-DOF underwater robot model is introduced below, and the corresponding positions of its coordinate system, $(O_0X_0Y_0Z_0)$ and the fixed coordinate system $(OXYZ)$, are given. Since the influence of the earth's rotation on low-speed moving objects is negligible, it is considered that the acceleration motion of objects on the earth's surface can be ignored. This is regarded as an inertial coordinate system $(O_0X_0Y_0Z_0)$, and Newton's laws of motion can be applied.

Due to its unique nature, it will be complicated to implement if the controller is designed using the 6-DOF model. Therefore, when creating the controller, the propeller design layout causes the vehicle not to have any lateral and vertical propellers to control its roll and heave motions, nor does it allow active control of the pitch and roll motions. Trajectory tracking management on the horizontal plane can generally be decomposed into two motion models, horizontal and vertical, thereby simplifying the AUV model. This paper only considers the motion of the AUV on the horizontal plane, that is, the lateral dynamics, including surge, sway, and yaw.

Newton's laws establish the kinematic equations in a fixed coordinate system [11]:

$$M\dot{v} + C(v)v + D(v)v + g(\eta) = F \tag{1}$$

where $F = [F_u, 0, F_r]$ are the surge force F_u and yaw moment F_r generated by the drive. Taking into account that balance is considered in the structural design of the robot, we can assume that the vehicle is symmetrical about the three planes $O_0X_0Y_0$, $O_0X_0Z_0$, and $O_0Y_0Z_0$, as is the inertia matrix, including the additional mass of the vehicle. $C(v)$ denotes the Coriolis and centripetal matrix having the following form: $F = [F_u, 0, F_r]$ where the surge force F_u and yaw moment F_r are generated by the drive. $C(v)$ represents Coriolis and the centripetal matrices of the form:

$$C(v) = \begin{bmatrix} 0 & 0 & -M_{\dot{v}}v \\ 0 & 0 & M_{\dot{u}}u \\ M_{\dot{v}}v & -M_{\dot{u}}u & 0 \end{bmatrix} \tag{2}$$

$D(v)$ is the damping matrix, which has the form:

$$D(v) = \begin{bmatrix} X_u + D_u|u| & 0 & 0 \\ 0 & Y_v + D_v|v| & 0 \\ 0 & 0 & N_r + D_r|r| \end{bmatrix} \tag{3}$$

$g(\eta)$ represents the restoring force composed of gravity and buoyancy.

$\dot{v} = \begin{bmatrix} \dot{u}\ \dot{v}\ \dot{r} \end{bmatrix}^T$ is the linear acceleration and angular acceleration of the object (motion) frame. $\dot{u}$ and $\dot{v}$ are linear accelerations in surge and sway direction, respectively. $\dot{r}$ is the angular acceleration in the yaw direction. $v = [u\ v\ r]^T$ are the linear and angular velocities relative to the object (motion) coordinate system, u—surge velocity, v—sway velocity, and r—yaw rate. $\eta = [x\ y\ \psi]^T$ are positions and orientations concerning the inertial (fixed) frame, x—surge position, y—sway position, and ψ—yaw angle.

The mass parameters of underwater vehicles are given at the beginning of the design: mass m and inertia I_z. For the additional mass of the underwater vehicle, it is necessary to use software to draw the AUV 3D model, and then use the fluid dynamics software to simulate it $X_{\dot{u}}, Y_{\dot{v}}, N_{\dot{r}}$. However, the viscous damping term $X_u, Y_v, N_r, X_{u|u|}, Y_{v|v|}, N_{r|r|}$ is difficult to obtain precisely, and may not even be available at all. Since the second-order viscous damping coefficient has little effect on the control system, this paper ignores $X_{u|u|}, Y_{v|v|}, N_{r|r|}$ in modeling.

The actual operation of an AUV needs its attitude and speed information when calculating the parameters required by the controller and the control force and torque. This information is generally obtained through the speed and position sensors carried by the AUV itself. Nevertheless, these data are based on the ground coordinate system, and the controller is designed according to the body coordinate system, so coordinate transformation is required. When calculating the pose and other parameters of the AUV based on the control force and moment, it is necessary to convert the control force and moment in the body coordinate system to the ground coordinate system. At this stage, Euler angles are used to describe the attitude of the underwater vehicle in the ground

coordinate system. The following gives the relationship between the object frame and the fixed frame at the linear velocity according to the literature:

$$\dot{\eta} = R(\psi)v \tag{4}$$

where $R(\eta)$ is the kinematic transformation matrix, and it is in the following form:

$$R(\psi) = \begin{bmatrix} \cos\psi & -\sin\psi & 0 \\ \sin\psi & \cos\psi & 0 \\ 0 & 0 & 1 \end{bmatrix} \tag{5}$$

According to the characteristics of the underwater vehicle system, the dynamic model is generalized, and a generalized mathematical model is obtained:

$$\begin{cases} m_1\dot{u} = -X_u u + m_2 vr + f_1(u,t) + F_u \\ m_2\dot{v} = -Y_v v - m_1 ur \\ m_3\dot{r} = -N_r r + (m_1 - m_2)uv + f_2(r,t) + F \end{cases} \tag{6}$$

where

$$m_1 = m - X_{\dot{u}},\ m_2 = m - Y_{\dot{v}},\ m_3 = I_z - N_{\dot{r}}$$

$f_1(u,t)$ and $f_2(r,t)$ represent the nonlinear perturbation of the marine environment to the underwater vehicle. The above equation shows that the underwater target vehicle has only two control inputs, which is a standard underactuated system. The mass m, and the viscous damping coefficient $[X_u, Y_v, N_r]$ are all positive numbers, and $\left[F_u, F_r, u, r, \dot{u}, \dot{v}\right]$ are bounded. Since the AUV is not driven in the sway direction, it is necessary to demonstrate the boundedness of the sway velocity v.

Let us define a Lyapunov function as:

$$V = \tfrac{1}{2}m_2 v^2 \tag{7}$$

Its first derivative is:

$$\begin{aligned} \dot{V} &= m_2 v\dot{v} \\ &= v(-Y_v v - m_1 ur + f_2(v,t)) \\ &= -Y_v v^2 - v m_1 ur + v f_2(v,t) \\ &< -Y_v v^2 + Q|v| \end{aligned} \tag{8}$$

where

$$Q = \max(|m_1 ur| + |f_2(v,t)|)$$

The following can be obtained: $\dot{V} \leqslant -\frac{1}{2}Y_v v^2, \forall |v| \geqslant \frac{2Q}{Y_v}$. Therefore, we can prove that the vehicle lateral motion speed v is stable and bounded.

3. Position Tracking Control Design

To simplify the expression, the established AUV actual dynamic model with a nonlinear random disturbance term is re-expressed as:

$$\begin{cases} \dot{u} = M_1(-X_u u + a_{11} vr + f_1(u,t) + F_u) \\ \dot{v} = M_2(-Y_v v + a_{22} ur) \\ \dot{r} = M_3(-N_r r + a_{33} uv + f_2(r,t) + F_r) \end{cases} \tag{9}$$

where

$$\begin{aligned} &M_1 = \tfrac{1}{m - X_{\dot{\mu}}},\ M_2 = \tfrac{1}{m - Y_{\dot{v}}},\ M_3 = \tfrac{1}{I_z - N_{\dot{r}}} \\ &a_{11} = m - Y_{\dot{v}},\ a_{22} = X_{\dot{\mu}} - m,\ a_{33} = Y_{\dot{v}} - X_{\dot{\mu}} \end{aligned}$$

The reference model needed in the MRAC system is the desired model, which is a reference model with the desired dynamic performance. This model is selected according to

the desired system dynamic performance index. The purpose of adaptive control is to make the output of the controlled system asymptotically follow the output of the specification (reference) model so that the system can meet the dynamic performance required by the system and finally make the output error (also called adaptive control error) asymptotically consistent and guaranteed to converges to zero. The control method proposed in this paper is shown in Figure 2.

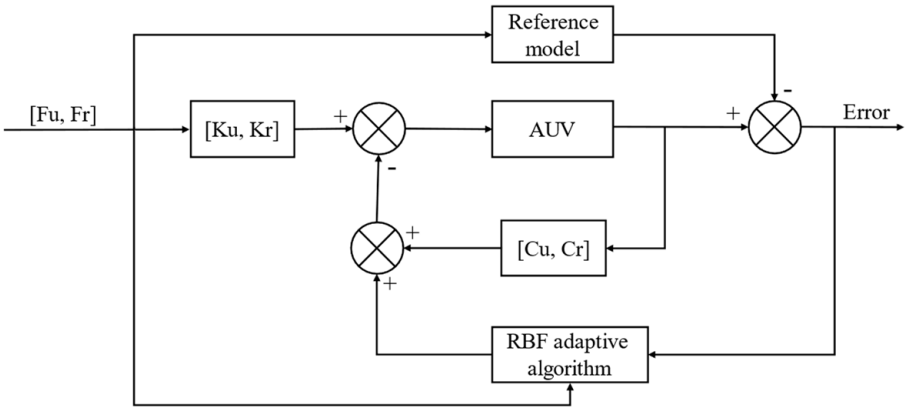


Figure 2. Schematic layout of MRAC.

The reference model of the MRAC system is obtained by discarding the nonlinear term in the existing AUV nonlinear dynamic model (10). The output of this model is the reference output for RBF-supervised training.

$$\begin{cases} \dot{u}_m = M_1(-X_u u_m + a_{11} v_m r_m + F_u) \\ \dot{v}_m = M_2(-Y_v v_m + a_{22} u_m r_m) \\ \dot{r}_m = M_3(-N_r r_m + a_{33} u_m v_m + F_r) \end{cases} \tag{10}$$

The trajectory tracking error is defined as:

$$\begin{cases} x_e = x - x_m \\ y_e = y - y_m \end{cases} \tag{11}$$

where x_m, y_m are the expected time-varying position coordinates. Through the (5) AUV kinematics equation, the dynamic equation of the position error can be obtained, and the velocity tracking error is given.

$$\begin{bmatrix} \dot{x}_e \\ \dot{y}_e \end{bmatrix} = \begin{bmatrix} \cos\psi & -\sin\psi \\ \sin\psi & \cos\psi \end{bmatrix} \begin{bmatrix} u \\ v \end{bmatrix} - \begin{bmatrix} \dot{x}_m \\ \dot{y}_m \end{bmatrix} \tag{12}$$

$$\begin{cases} e_u = u - u_m \\ e_v = v - v_m \end{cases} \tag{13}$$

Because biological neurons have local responses, some researchers introduced RBF into the neural network design, resulting in an RBF neural network. And, it is found that an RBF neural network has good approximation performance to nonlinear continuous functions. Since the RBF network has only one hidden layer, the control effect is excellent, and it is easier to deploy in controllers and computing modules with low computing power.

$R_j(x)$ is the radial basis function, $j = 1, 2, 3, \ldots, n$.

The input of the RBF network is $x = [x_1(k), x_2(k), \cdots x_n(k)]^T$, so the number of nodes in the input layer is n. The AUV system input has the surge force F_u and yaw moment F_r. The two propellers installed at the tail can simultaneously provide horizontal force and moment, so the horizontal and surge forces are controlled separately. Since the calculation

process of the two networks is relatively similar, only the controller design process related to the horizontal force is given in this article.

The output of RBF is $y_m(k)$, and the activation function of the hidden layer is the Gaussian kernel function, also known as the radial basis (RBF) function, which is a scalar function symmetrical along the radial direction, which is used to map finite-dimensional data to high-dimensional space, in the form:

$$R_j(x) = exp\left(-\frac{\|x-c_j\|^2}{2b_j^2}\right), j = 1, 2, \cdots, n \tag{14}$$

where c_j is the center point of the j basis function, and $c_j = \left[c_{j1}, c_{j2}, \cdots, c_{jn}\right]^T$. b_j is a parameter that can be set manually, determining the width of the Gaussian function around the center point. m is the number of nodes in the hidden layer, and m determines the control effect of the controller and the calculation power required to be provided by the calculation module. Therefore, selecting an appropriate number of hidden layer nodes is imperative.

The derivative of the activation function is:

$$\begin{aligned} \frac{\partial R_j(x)}{\partial b_j} &= exp\left(-\frac{\|x-c_j\|^2}{b_j^2}\right)\frac{\|x-c_j\|^2}{b_j^3} = R_j(x)\frac{\|x-c_j\|^2}{b_j^3} \\ \frac{\partial R_j(x)}{\partial c_{ji}} &= exp\left(-\frac{\|x-c_j\|^2}{b_j^2}\right)\frac{(x_i-c_{ji})}{b_j^2} = R_j(x)\frac{(x_i-c_{ji})}{b_j^2} \end{aligned} \tag{15}$$

The RBF training consists of the input signal's forward propagation and the error's back propagation process.

P-1: The input signal (horizontal force provided by the propeller of the AUV) is propagated forward, and the output of the RBF network is calculated.

The output of the neurons in the input layer is $x = [x_1(k), x_2(k), \ldots, x_n(k)]^T$, and (14) is used to obtain the hidden layer neuron. The output of meta is:

$$\begin{gathered} R_j(x(k)) = exp\left(-\frac{\|x(k)-c_j(k-1)\|^2}{b_j^2(k-1)}\right) \\ j = 1, 2, \cdots, n \end{gathered} \tag{16}$$

The input to the neurons in the output layer is:

$$y_m(k) = \sum_{m}^{j=1} w_j(k-1)R_j(x(k)) \tag{17}$$

where $w_j(k-1)$ is the weight from the j hidden layer neuron to the output layer neuron at $(k-1)$ time:

$$e(k) = y(k) - y_m(k) \tag{18}$$

where $y(k)$ is the system's actual output and $y_m(k)$ is the output of the reference model.

The performance indicator function can be introduced:

$$E(k) = \frac{1}{2}e^2(k) \tag{19}$$

P-2: Error backpropagation. The δ learning algorithm is used to adjust the weights between the layers of the RBF network, ensuring that AUVs adapt to time-varying disturbances.

According to the gradient descent method, the weight learning algorithm is as follows:

The weight from the hidden layer to the output layer is $w_j(k)$.

From (18) and (19) we can obtain:

$$\delta^{(2)} = \frac{\partial E(k)}{\partial y_m(k)} = \frac{\partial E(k)}{\partial e(k)}\frac{\partial e(k)}{\partial y_m(k)} = -e(k) \tag{20}$$

From (17) and (20) we can obtain:

$$\frac{\partial E(k)}{\partial w_j(k-1)} = \frac{\partial E(k)}{\partial y_m(k)} \frac{\partial y_m(k)}{\partial w_j(k-1)} = \delta^{(2)} R_j(x(k)) = -e(k) R_j(x(k)) \tag{21}$$

Therefore, the learning algorithm of the weight $w_j(k)$ from the hidden layer to the output layer is:

$$\triangle w_j(k) = -\eta \frac{\partial E(k)}{\partial w_j(k-1)} = \eta e(k) R_j(x(k)) \tag{22}$$

$$w_j(k) = w_j(k-1) + \nabla w_j(k) + \alpha\big(w_j(k-1) - w_j(k-2)\big) \tag{23}$$

where η is the learning rate ($\eta > 0$) and α is the momentum factor ($\alpha \in [0, 1)$).

The hidden-layer Gaussian function parameters are $b_j(k)$ and $c_{ji}(k)$.

From (20) and (17) we can obtain:

$$\delta_j^{(1)} = \frac{\partial E(k)}{\partial R_j(x(k))} = \frac{\partial E(k)}{\partial y_m(k)} \frac{\partial y_m(k)}{\partial R_j(x(k))} = \delta^{(2)} w_j(k-1) \tag{24}$$

Then, we can use (24) and (15) to obtain:

$$\begin{aligned} \frac{\partial E(k)}{\partial b_j(k-1)} &= \frac{\partial E(k)}{\partial R_j(x(k))} \frac{\partial R_j(x(k))}{\partial b_j(k-1)} = -e(k) w_j(k-1) R_j(x(k)) \frac{x(k) - c_j(k-1)^2}{b_j^3(k-1)} \\ \frac{\partial E(k)}{\partial c_{ji}(k-1)} &= \frac{\partial E(k)}{\partial R_j(x(k))} \frac{\partial R_j(x(k))}{\partial c_{ji}(k-1)} = -e(k) w_j(k-1) R_j(x(k)) \frac{x(k) - c_{ji}(k-1)}{b_j^2(k-1)} \end{aligned} \tag{25}$$

Then, the learning algorithm of $b_j(k)$ and $c_{ji}(k)$ is:

$$\begin{aligned} \nabla b_j(k) &= -\eta \frac{\partial E(k)}{\partial b_j(k-1)} = \eta e(k) w_j(k-1) R_j(x(k)) \frac{x(k) - c_j(k-1)^2}{b_j^3(k-1)} \\ b_j(k) &= b_j(k-1) + \nabla b_j(k) + \alpha\big(b_j(k-1) - b_j(k-2)\big) \\ \nabla c_{ji}(k) &= -\eta \frac{\partial E(k)}{\partial c_{ji}(k-1)} = \eta e(k) w_j(k-1) R_j(x(k)) \frac{x_i(k) - c_{ji}(k-1)}{b_j^2(k-1)} \\ c_{ji}(k) &= c_{ji}(k-1) + \nabla c_{ji}(k) + \alpha\big(c_{ji}(k-1) - c_{ji}(k-2)\big) \end{aligned} \tag{26}$$

4. Stability Analysis

It should be noted that the control scheme in this section is based on the assumption that all states are measurable and feedback is available.

Define the desired surge and sway speeds.

$$\begin{bmatrix} u_d \\ v_d \end{bmatrix} = \overline{\Gamma_h} \begin{bmatrix} \dot{x}_d + l_x \tanh\left(-\frac{k_x}{l_x} x_e\right) \\ \dot{y}_d + l_y \tanh\left(-\frac{k_y}{l_y} y_e\right) \end{bmatrix} \tag{27}$$

where

$$\overline{\Gamma_h} = \begin{bmatrix} cos\psi & sin\psi \\ -sin\psi & cos\psi \end{bmatrix}$$

k_x, k_y, l_x, l_y are constants, and $k_x, k_y > 0, l_x, l_y \neq 0$.

Bring in Formulas (13) and (27), and the result is as follows:

$$\begin{bmatrix} e_u \\ e_v \end{bmatrix} = \overline{\Gamma_h} \begin{bmatrix} \dot{x}_e - l_x \tanh\left(-\frac{k_x}{l_x} x_e\right) \\ \dot{y}_e + l_y \tanh\left(-\frac{k_y}{l_y} y_e\right) \end{bmatrix} \tag{28}$$

$\left|\overline{\Gamma_h}\right| = 1$, the matrix is non-singular. When the speed error e_u, e_v converges to 0, it can be guaranteed.

$$\begin{aligned} \dot{x}_e &= l_x \tanh\left(-\frac{k_x}{l_x} x_e\right) \\ \dot{y}_e &= l_y \tanh\left(-\frac{k_y}{l_y} y_e\right) \end{aligned} \tag{29}$$

Based on the Lyapunov stability theory, the adaptive controller is referenced according to the AUV motion Equation (6) and the RBF-based model (Figure 2). The AUV trajectory tracking error and velocity error are asymptotically stable. Let V represent the Lyapunov function. If the following conditions are met, the actual curve tracks the upper expected curve ($\chi = \chi_m$), that is, the actual system output is equal to the reference model system output. Then, it shows that the trajectory tracking error is asymptotically stable. Furthermore, the equilibrium point of the closed-loop system at the origin is globally asymptotically stable according to the probability.

The system output error predicted by the neural network, that is, the output of the neural network, is:

$$y = w_f h_f \tag{30}$$

The actual error encountered by the AUV during operation is:

$$y = w_f h_f + \delta_e \tag{31}$$

Let us define a Lyapunov function:

$$V = \tfrac{1}{2}(x - x_m)^2 + (y - y_m)^2 \tag{32}$$

Taking the derivative of the Lyapunov function and substituting (29) into it gives:

$$\dot{V} = x_e \dot{x}_e + y_e \dot{y}_e = -x_e l_x \tanh\left(\frac{k_x}{l_x} x_e\right) - l_y y_e \tanh\left(\frac{k_y}{l_y} y_e\right) \tag{33}$$

It can be concluded from the above formula that when $(x_e, y_e) \neq 0$, $k_x, k_y > 0$, and l_x, $l_y \neq 0$, $\dot{V}_1 < 0$, it can be explained that (x_e, y_e) in this case gradually converge to $(0, 0)$.

5. Actual Tracking Test and Verification of AUV

The experimental simulation data. According to the RBF function method proposed in this paper, use Algorithm 1 to test the tracking performance of the underwater robot on the horizontal plane. After several experiments and simulation tests, the more rational RBF system parameters are provided, including the node number of the input layer $n = 1$, the node number of the hidden layer $h = 30$, the learning rate $\eta = 0.08$, and the momentum factor $\alpha = 0.002$. In addition, the AUV experiment is designed to verify the AUV trajectory tracking ability. The control algorithm designed in this paper is downloaded to the AUV electronic bin shown in Figure 3, and the underwater vehicle designed in Figure 4 is used to conduct the underwater search cable experiment.

Algorithm 1: RBF-based MRAC

Known nonlinear system structure parameters, such as n_y, n_u, d, etc.

1. Input the initial data of the system, set the initial value of RBF network parameters $b_j(0)$, $c_{ji}(0)$, and $w_j(0)$, and other parameters such as the number of hidden layer neurons h, learning rate η, momentum factor α, etc.;
2. Sample the actual system output $y(k)$, and calculate the current network output $y_m(k)$ using Formulas (16) and (17);
3. Use Formulas (22) and (26) to calculate the network parameter increment $\nabla w_j(k)$, $\nabla b_j(k)$, and $\nabla c_{ji}(k)$;
4. Use Formulas (23) and (25) to calculate the network parameters $w_j(k)$, $b_j(k)$, and $c_{ji}(k)$;
5. Use Step 2 $(k \to k+1)$ to continue the cycle.

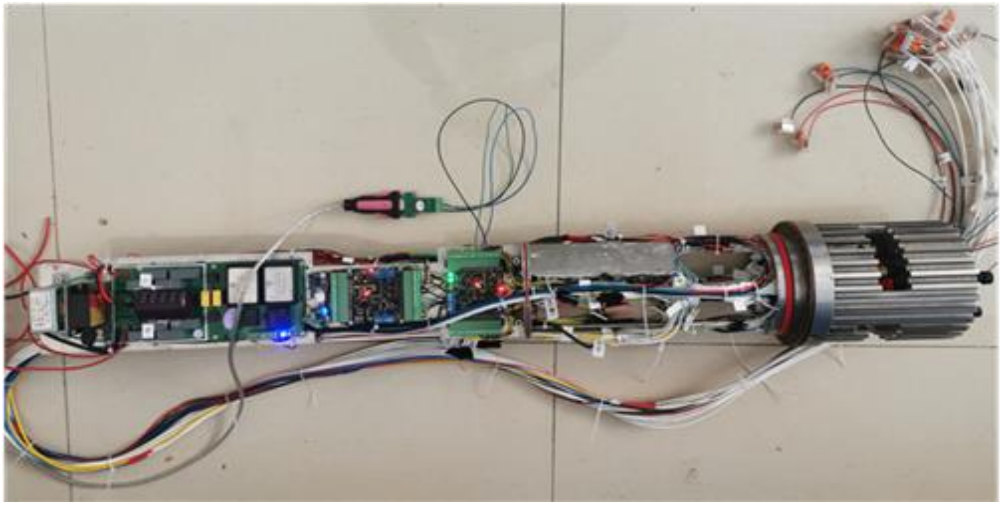


Figure 3. Electronic warehouse for underwater robots.



Figure 4. Typical AUV Model.

5.1. RBF-Based MRAC

Two time-varying functions are used as the input of the AUV control terminal. They are, respectively, the surge force F_u and the yaw moment F_r generated by the actuator.

$$\begin{aligned} F_u &= 10\sin(3t + 0.1) \\ F_r &= 6sin(0.4t + 2) - 0.2 \end{aligned} \tag{34}$$

This simulation mainly considers the tracking performance in the surge direction. For a more intuitive understanding, the environmental disturbance in the nonlinear continuity equation is set as:

$$\begin{aligned} f_1(u,t) &= 1000sin(0.02t) \\ f_2(r,t) &= 0 \end{aligned} \tag{35}$$

The underwater robot used for testing is shown in Figure 1, with mass $m = 20.32$ kg and inertia $I_z = 2.3\ \mathrm{kg} \cdot \mathrm{m}^2$. The 3D model of the underwater robot is imported into the hydrodynamic analysis software to obtain the hydrodynamic additional mass, $X_\mu = -0.62$ kg/s, $Y_v = -23.6667$ kg/s, $N_r = -23.6667\ \mathrm{kg} \cdot \mathrm{m}^2/\mathrm{s}$. The speed and acceleration of the robot can be obtained through its sensors, which are convenient for real-time control. The following

nonlinear dynamic model is used as the actual model of the MRAC controller. Of course, the reference model is to remove the nonlinear disturbance $f_1(u,t,)$ and $f_2(r,t)$ in (9):

$$\begin{aligned} \dot{u} &= M_1(5.871u + 43.9867vr + f_1(u,t) + F_u) \\ \dot{v} &= M_2(43.6971v - 20.94ur) \\ \dot{r} &= M_3(23.6667r - 23.0467uv + f_2(r,t) + F_r) \end{aligned} \tag{36}$$

where

$$M_1 = 0.0478, M_2 = 0.00.0227, M_3 = 0.0385$$

Experiments are carried out according to the above conditions, and the nonlinear disturbance given by Formula (35) is applied. The initial conditions are $x_0 = 1m$ and $y_0 = 0.6m$. The experiment is carried out in a pool that can provide waves, which can effectively simulate the complex underwater environment and increase the uncertainty of the model. The data obtained by the built-in acceleration sensor of the AUV is compared with the expected trajectory value for analysis. The experimental results are shown in Figures 5 and 6. Figure 6 shows the output of the sway direction controller and the output of the reference model. Figure 7 shows the controller output and desired output for the yaw rate. It can be found that the proposed RBF and model reference adaptive controller can achieve the desired output within a certain period when the AUV has disturbance (underwater flow, etc.) uncertainty. It can make $\lim_{t\to\infty} error = 0$. Using the controller designed in this article, the underwater robot is controlled for trajectory tracking experiments. It is verified that the AUV can effectively track the preset trajectory in the presence of water flow (Figure 7).

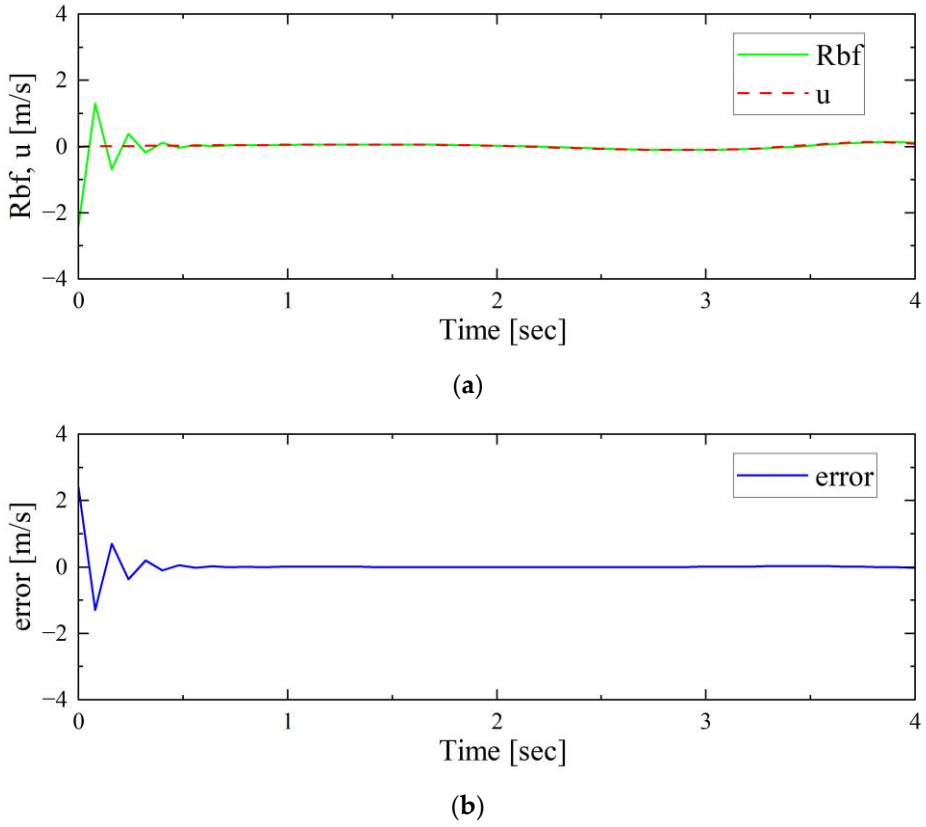


Figure 5. (**a**) Surge speed control output and desired output. (**b**) Error.

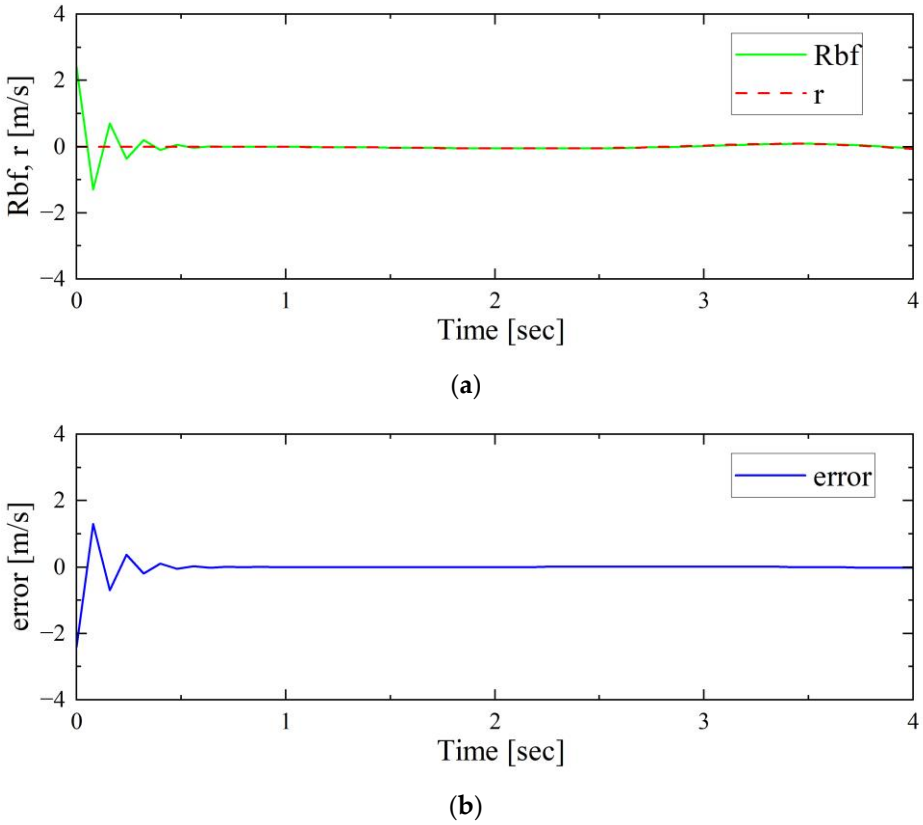


Figure 6. (**a**) Yaw angular velocity controller output and desired output. (**b**) Error.



Figure 7. An AUV experiment.

5.2. PID Control

The simulation results using PID control in the presence of water flow are shown in Figure 8. The initial conditions are $x_0 = 1m$, $y_0 = 0.6m$, and the parameters of PID are: $[p = 0.1, i = 0.5, d = 0.8]$. We compared the control effect of the RBF method and PID. Due to the strong coupling of AUV system parameters, the PID controller cannot drive the AUV to the desired trajectory within a certain period. The initial values of the two methods are set the same, and the designed RBF controller can reduce the vibration convergence time of the underwater robot to zero in the presence of underwater interference for the AUV. Moreover, the vibration amplitude of the robot reduces when it moves underwater. Therefore, the effectiveness of our proposed control strategy can be verified.

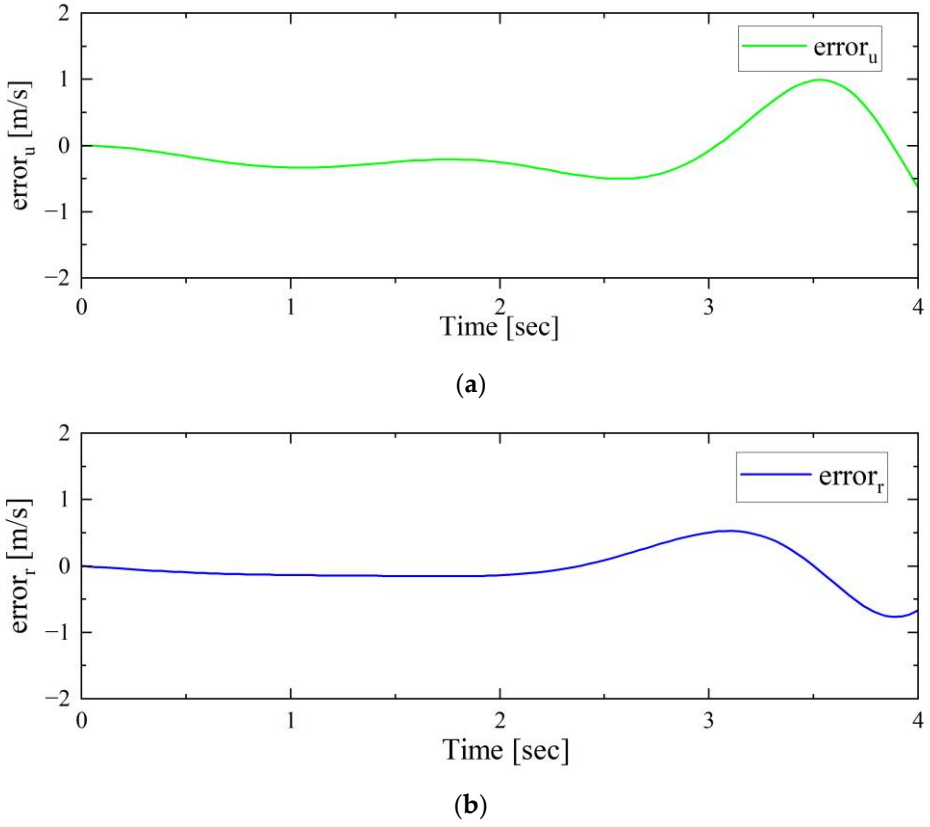


Figure 8. (**a**) PID controller surge speed error. (**b**) PID controller yaw angular velocity error.

6. Discussion

This paper proposed a nonlinear AUV system which was a horizontal plane model. The AUV system always has uncertain disturbances and nonlinear terms. For the under-actuated AUV model, the sway velocity's boundedness was verified by the Lyapunov function. The entire controller was a closed-loop that was combined with the RBF neural network where the tracking error of the AUV was less than 1%. The stabilization time of the backstepping control strategy (Figure 5) proposed in the literature [28] was more than 5 s, while the stabilization time of the controller proposed in this paper was 0.64 s, which is a significant improvement compared with the literature. This designed controller was simulated for analyzing the position of the tracking control model and the actuator's position of the AUV. Finally, the AUV trajectory diagram using the PID controller experiments was given as a comparison, and the stability of the AUV controller was demonstrated. However, there is no accurate model for most actuators in the actual research; even some actuator parts will be changed during operation.

Given the analysis, it can be found that the model of the actuators is time-varying or uncertain. It is a change for model-depended control methods applied in mechanisms. Therefore, it is necessary to study the controlling systems whose model is time-invariant or easy to determine.

Author Contributions: Data curation, Q.Z.; formal analysis, L.G. and Q.Z.; investigation, Q.Z.; methodology, L.G. and X.T.; resources, L.G. and X.T; supervision, M.A.H.S. and X.T.; writing—review and editing, Q.Z. All authors have read and agreed to the published version of the manuscript.

Funding: This work was supported by the Key R&D Program of Zhejiang Province (No.2021C03013), and the Fundamental Research Funds for the Provincial Universities of Zhejiang (No. GK229909299001-007).

Institutional Review Board Statement: Not applicable.

Informed Consent Statement: Not applicable.

Data Availability Statement: Not applicable.

Conflicts of Interest: The authors declare no conflict of interest.

References

1. Vu, M.T.; Le Thanh, H.N.N.; Huynh, T.T.; Thang, Q.; Duc, T.; Hoang, Q.D.; Le, T.H. Station-keeping control of a hovering over-actuated autonomous underwater vehicle under ocean current effects and model uncertainties in horizontal plane. *IEEE Access* **2021**, *9*, 6855–6867. [CrossRef]
2. Walker, K.L.; Gabl, R.; Aracri, S.; Cao, Y.; Stokes, A.A.; Kiprakis, A.; Giorgio-Serchi, F. Experimental validation of wave induced disturbances for predictive station keeping of a remotely operated vehicle. *IEEE Robot. Autom. Lett.* **2021**, *6*, 5421–5428. [CrossRef]
3. Carreras, M.; Hernández, J.D.; Vidal, E.; Palomeras, N.; Ribas, D.; Ridao, P. Sparus II AUV—A hovering vehicle for seabed inspection. *IEEE J. Ocean. Eng.* **2018**, *43*, 344–355. [CrossRef]
4. Khan, N.S.; Humphries, U.W.; Kumam, W.; Kumam, P.; Muhammad, T. Dynamic pathways for the bioconvection in thermally activated rotating system. *Biomass Convers. Biorefin.* **2022**. [CrossRef]
5. Khan, N.S.; Hussanan, A.; Kumam, W.; Kumam, P.; Suttiarporn, P. Accessing the thermodynamics of Walter-B fluid with magnetic dipole effect past a curved stretching surface. *ZAMM-J. Appl. Math. Mech./Z. Für Angew. Math. Mech.* **2023**, E202100112. [CrossRef]
6. Peng, Y.; Guo, L.; Meng, Q. Backstepping Control Strategy of an Autonomous Underwater Vehicle Based on Probability Gain. *Mathematics* **2022**, *10*, 3958. [CrossRef]
7. Serrani, A.; Conte, G. Robust nonlinear motion control for AUVs. *IEEE Robot. Autom. Mag.* **1999**, *6*, 33–38. [CrossRef]
8. Sedghi, F.; Arefi, M.M.; Abooee, A.; Kaynak, O. Adaptive robust finite-time nonlinear control of a typical autonomous underwater vehicle with saturated inputs and uncertainties. *IEEE/ASME Trans. Mechatron.* **2020**, *26*, 2517–2527. [CrossRef]
9. Kim, H.H.; Lee, M.C.; Cho, H.J.; Hwang, J.H.; Won, J.S. SMCSPO-Based Robust Control of AUV in Underwater Environments including Disturbances. *Appl. Sci.* **2021**, *11*, 10978. [CrossRef]
10. Shi, Y.; Shen, C.; Fang, H.; Li, H. Advanced control in marine mechatronic systems: A survey. *IEEE/ASME Trans. Mechatron.* **2017**, *22*, 1121–1131. [CrossRef]
11. Sangalang, R.G.B.; Masangcay, D.J.S.; Torino, C.M.R.; Gutierrez, D.J.C. Design of a control architecture for an underwater remotely operated vehicle (ROV) used for search and rescue operations. *Kybernetika* **2022**, *58*, 237–253. [CrossRef]
12. Sheida, K.; Nobari, M.; Baigzadehnoe, B.; Bevrani, H. An Artificial Bee Colony Based PID Controller for Depth Control of an Autonomous Underwater Vehicle. In Proceedings of the International Conference on Control, Instrumentation and Automation (ICCIA), Tehran, Iran, 2–3 March 2022; pp. 1–6.
13. Santhakumar, M.; Asokan, T. Investigations on the dynamic station keeping of an underactuated autonomous underwater robot. *Int. J. Simul. Model.* **2011**, *10*, 145–157. [CrossRef]
14. Ferdaus, M.M.; Pratama, M.; Anavatti, S.G.; Garratt, M.A.; Lughofer, E. PAC: A novel self-adaptive neuro-fuzzy controller for micro aerial vehicles. *Inf. Sci.* **2020**, *512*, 481–505. [CrossRef]
15. Hady, M.A.; Kocer, B.B.; Kandath, H.; Pratama, M. Real-time uav complex missions leveraging self-adaptive controller with elastic structure. *arXiv* **2019**, arXiv:1907.08619.
16. Wang, X.; Abtahi, S.M.; Chahari, M.; Zhao, T. An adaptive neuro-fuzzy model for attitude estimation and control of a 3 DOF system. *Mathematics* **2022**, *10*, 976. [CrossRef]
17. Yan, F.; Hou, X.; Tian, T. Fractional-order multivariable adaptive control based on a nonlinear scalar update law. *Mathematics* **2022**, *10*, 3385. [CrossRef]
18. Li, H.; Shi, Y. *Robust Receding Horizon Control for Networked and Distributed Nonlinear Systems*; Springer International Publishing: Cham, Switzerland, 2017.
19. Li, H.; Shi, Y.; Yan, W. On neighbor information utilization in distributed receding horizon control for consensus-seeking. *IEEE Trans. Cybern.* **2015**, *46*, 2019–2027. [CrossRef]
20. Shen, C.; Shi, Y.; Buckham, B. Trajectory tracking control of an autonomous underwater vehicle using Lyapunov-based model predictive control. *IEEE Trans. Ind. Electron.* **2017**, *65*, 5796–5805. [CrossRef]
21. Mehrez, M.W.; Worthmann, K.; Cenerini, J.P.; Osman, M.; Melek, W.W.; Jeon, S. Model predictive control without terminal constraints or costs for holonomic mobile robots. *Robot. Auton. Syst.* **2020**, *127*, 103468. [CrossRef]
22. Di Carlo, J.; Wensing, P.M.; Katz, B.; Bledt, G.; Kim, S. Dynamic locomotion in the mit cheetah 3 through convex model-predictive control. In Proceedings of the 2018 IEEE/RSJ International Conference on Intelligent Robots and Systems (IROS), Madrid, Spain, 1–5 October 2018; pp. 1–9.
23. Chen, H.; Allgöwer, F. A quasi-infinite horizon nonlinear model predictive control scheme with guaranteed stability. *Automatica* **1998**, *34*, 1205–1217. [CrossRef]
24. Yuh, J. A neural net controller for underwater robotic vehicles. *IEEE J. Ocean. Eng.* **1990**, *15*, 161–166. [CrossRef]
25. Zhang, J.; Xiang, X.; Zhang, Q.; Li, W. Neural network-based adaptive trajectory tracking control of underactuated AUVs with unknown asymmetrical actuator saturation and unknown dynamics. *Ocean. Eng.* **2020**, *218*, 108193. [CrossRef]
26. Seshagiri, S.; Khalil, H.K. Output feedback control of nonlinear systems using RBF neural networks. *IEEE Trans. Neural Netw.* **2000**, *11*, 69–79. [CrossRef] [PubMed]

27. Butler, H. *Model Reference Adaptive Control: From Theory to Practice*; Prentice-Hall, Inc.: Saddle River, NJ, USA, 1992.
28. Peng, Y.; Guo, L.; Meng, Q.; Chen, H. Research on hover control of AUV uncertain stochastic nonlinear system based on constructive backstepping control strategy. *IEEE Access* **2022**, *10*, 50914–50924. [CrossRef]

Disclaimer/Publisher's Note: The statements, opinions and data contained in all publications are solely those of the individual author(s) and contributor(s) and not of MDPI and/or the editor(s). MDPI and/or the editor(s) disclaim responsibility for any injury to people or property resulting from any ideas, methods, instructions or products referred to in the content.